Electronic Supplementary Material (ESI) for Journal of Materials Chemistry A.
This journal is © The Royal Society of Chemistry 2020

Supporting Information

"Fiber-in-tube" Hierarchical Nanofiber Based on Defective Bimetal Oxide@C Hollow Bubbles: A High-Efficiency and High-Performance Cathode for Hybrid Zn Battery

Yang Zhou[a], Yu Song[b], Sen Zhang[b,*] and Chao Deng[a,*]

[1] Key Laboratory for Photonic and Electronic Bandgap Materials, Ministry of Education; College of Chemistry and Chemical Engineering, Harbin Normal University, Harbin, 150025, Heilongjiang, China

[2] College of Material Science and Chemical Engineering, Harbin Engineering University, Harbin 150001, Heilongjiang, China

* Corresponding author: S. Zhang, C. Deng

E-Mail: senzhang@hrbeu.edu.cn (S. Zhang)

chaodenghsd@sina.com (C. Deng)

Part I: Experimental details, Calculations & Discussions

S-1-1: Preparation of the DBHF nanofiber

i) Preparation of the precursor

Firstly, the precursor was prepared by an electrospinning technique. The precursor solution for electrospinning is prepared by dissolving the nickel acetate, cobalt acetate and PAN (MW: 150000) in the N, N-dimethylformamide (DMF) with vigorously stringing over night. The prepared solution was loaded into a plastic syringe equipped with a stainless nozzle syringe. The solution was then ejected on to a drum collected covered with aluminum foil. The distance between the needle and the rotating drum collector was ~12 cm and a high voltage of 15 kV was applied on between the collector and the syringe tip. After the electrospinning process, the film was peeled off from the collector and the precursor was achieved.

ii) Preparation of the DBHF nanofiber

The prepared electrospun precursor was firstly stabilized at 280 ^{o}C in air. Then the resultant product was calcinated at 600 ^{o}C in the N_2 atmosphere with an ultrafast heating rate of 250 ^{o}C/min. After that, the resultant product is quickly quenched to the low temperature through inserting into liquid nitrogen to achieve the intermediate product. Finally, the resultant intermediate product was retreated in air to achieve the final product.

S-1-2: Synthesis of reference samples

Two reference samples with adjusted synthetic conditions were prepared for comparison.

i) For the preparation of the NIR reference sample, the electrospun precursor was firstly stabilized at 280 ^{o}C in air. Then the resultant product was calcinated at 600 ^{o}C in the N_2 atmosphere with a slow heating rate of 2 ^{o}C/min. Then the resultant intermediate product was retreated in air to achieve the final product.

ii) For the preparation of the HS reference sample, the electrospun precursor was stabilized at 280 ^{o}C in air. Then the resultant product was calcinated at 600 ^{o}C in the air.

S-2: Materials characterizations

Powder X-ray diffraction (XRD, Bruker D8/Germany) using Cu Kα radiation was employed to identify the crystalline phase of the material. The experiment was performed by using step mode with a fixed time of 3 *s* and a step size of 0.02^{o}. The XRD pattern was refined by using the Rietveld method. The morphology was observed with a scanning electron microscope (SEM, HITACHIS-4700) and a transmission electron microscope (TEM, JEOS-2010 PHILIPS). The element distribution of the sample was confirmed by energy dispersive X-ray detector (EDX). X-ray photoelectron spectroscopy (XPS, Thermo ESCALAB 250) was employed to measure the chemical or electronic state of each element. Thermogravimetric analysis (TGA, NETZSCH STA 449C) was used to investigate the carbon content of the sample. Nitrogen adsorption-desorption isotherms were measured using a Micromeritics ASAP 2010. Specific surface area was calculated using the Brunauer-Emmett-Teller (BET) method.

S-3: Electrochemical measurements

S-3-1 Evaluation of the ORR/OER catalytic properties

The electrochemical measurements were conducted on a rotating electrode system (Pine Inc.) with a CHI electrochemical workstation at room temperature. A three-electrode system was used with a glassy carbon rotating disk electrode (5 mm in diameter) with fixed nanofibers as the working electrode, a platinum plat as the counter electrode and the an Ag/AgCl electrode as the reference electrode. The 0.1 M KOH solution was used as electrolyte. All the potentials were transferred into the reversible hydrogen electrode (RHE) form according to the Nernst equation.

$$E_{RHE} = E_{Ag/AgCl} + 0.059 \times pH + 0.21V \quad (1)$$

For the ORR experiments, pure oxygen was purged in the electroyte for 30 minutes before the tests and the oxygen tube was maintained in the headspace of the electrolyte through the test process. Prior to cyclic voltammetry (CV) and linear sweep voltammetry (LSV) measurements, the working electrodes were activated by CV tests at a sweep rate of 50 mV s^{-1}. Linear sweep voltammetry (LSV) for ORR polarization curves was conducted using various rotating speeds from 400 to 2500 rpm at a scan rate of 5 mV s^{-1} from 0.2 to 1.1 V versus RHE. The Koutecky-Levich equation can be used to determine the electron transfer number (n):

$$j^{-1} = j_k^{-1} + j_d^{-1} \quad (2)$$

Where j is the measured current density and j_k and j_d are the kinetic and diffusion limiting current densities, respectively.

$$j_d = 0.2nFD_O^{2/3}v^{-1/6}C_{O_2}w^{1/2} \quad (3)$$

$$j_k = nFkC_{O_2} \quad (4)$$

Where ω is the angular velocity (rpm), n is the transferred electron number, F is the Faraday constant, D_{O2} is the diffusion coefficient of O_2 in 0.1 M KOH, v is the knetmatic viscosity, and C_{O2} is the bulk concentration of O_2.

LSV for OER polarization curves was conducted using 1600 rpm at a scan rate of 5 mV s^{-1} from 1.1 to 1.8 V versus RHE.

S-3-2 Evaluation of the Zn-ion battery performance

The properties of Zn-ion battery were measured in a two-electrode system with the prepared nanofibers film as the working electrode and the Zn plate as the counter electrode. The galvanostatic charge/discharge tests were conducted on a LAND battery testing system (Wuhan, China).

S-3-3 Electrochemical performance of the liquid hybrid Zn battery

The liquid hybrid Zn battery was assembled in a home-built cell. The prepared nanofibers were treated with PTFE to improve hydrophobicity and create gas transport pathways to increase triple phase boundaries. Then the treated nanofibers were used as the cathode, the polished Zn plate were used as anode and the mixed solution of 6 KOH and 0.2 M zinc acetate was used as electrolyte. The cyclic voltammetry (CV) were measured in a CHI electrochemical workstation, and the galvanostatic charge/discharge tests were conducted on a LAND battery testing system (Wuhan, China).

S-4 Fabrication and electrochemical measurements of flexible hybrid Zn-ion battery

S-4-1 Synthesis of the Zn nanosheet@CNTF fiber anode

Zn nanosheets were grown on the CNTF by electrodeposition at room temperature employing the CHI 760 electrochemical work station. The electrodeposition was carried

out in a three-electrode configuration with the textile as working electrode, a Pt wire as counter electrode and a saturated calomel electrode (SCE) as reference electrode. The mixed solution of $ZnSO_4 \cdot 7H_2O$, Na_2SO_4 and H_3BO_3 was used as electrolyte. The electrodeposition was conduct at -40 mA cm^{-2} at room temperature. Then the resultant electrode was washed with DI water and dried in a vacuum oven at 60 ^oC for 12 hours.

S-4-2 Preparation of hydrogel electrolyte

The hydrogel electrolyte was prepared according to the process reported in previous reports [S1,S2]. Firstly, the concentrated sodium hydroxide solution was slowly dropped into an aqueous solution of acrylic acid monomer with continuously stirring in ice-bath. Next, the initiator of ammonium persulphate was added to the mixed solution, which was followed by the crosslinker of N, N'-methylene diacrylamide. Then mixture was placed in an over at 65 ^oC to free-radical polymerization. Finally, the product was peeled off and dried in an over. After fully soaking in the mixed electrolyte of potassium hydroxide and zinc acetate to achieve the equilibrate state, the hydrogel electrolyte was prepared.

S-4-3 Fabrication of flexible hybrid Zn battery

The nanofibers were used as the cathode, the Zn nanosheet@carbon cloth as anode the phydrogel was used as electrolyte. Both electrodes were paved on each side of the hydrogel film under ambient conditions. Therefore, the hydrogel electrolyte can also be used as the separator in the flexible solid state batteries.

Part II: Supporting Figures

Figure S1

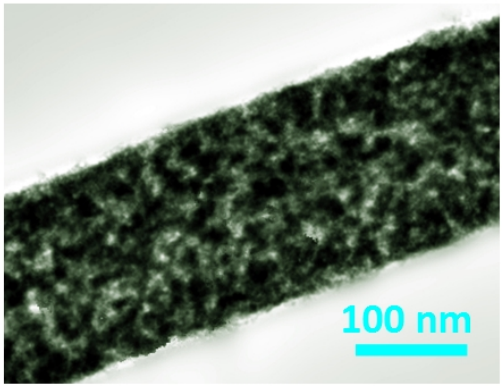

Figure S1 TEM image of the intermediate product for the NIR sample.

Figure S2

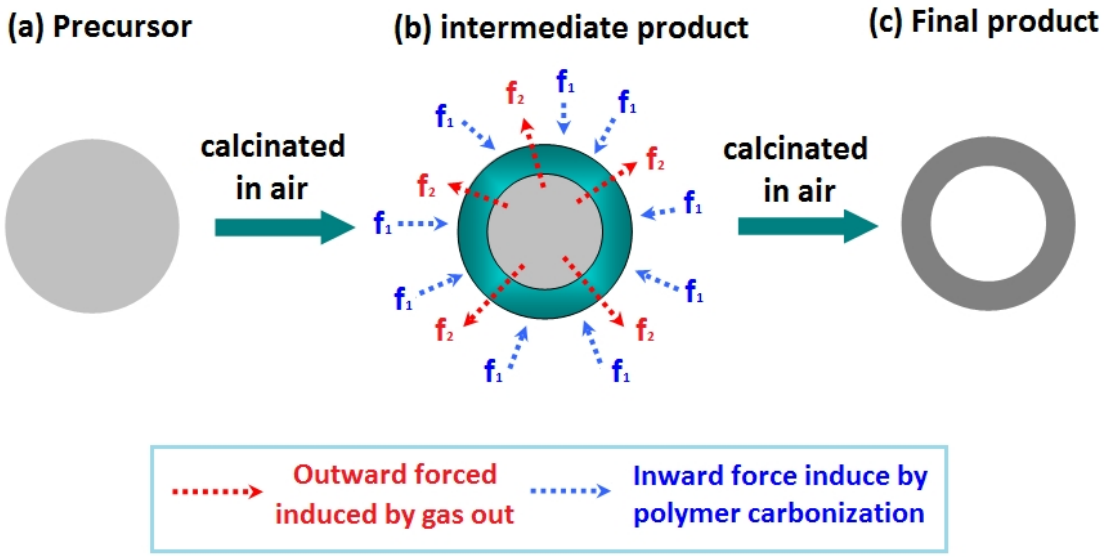

Figure S2 Schematic illustration of the formation process during calcination in air. a is the electrospinning precursor; b is the intermediate product during calcination; c is the final product after calcination. f_1 is the inward forces induced by the polymer carbonation; f_2 is the outward forces induced by the gas out generated from the combustion reaction.

Figure S3

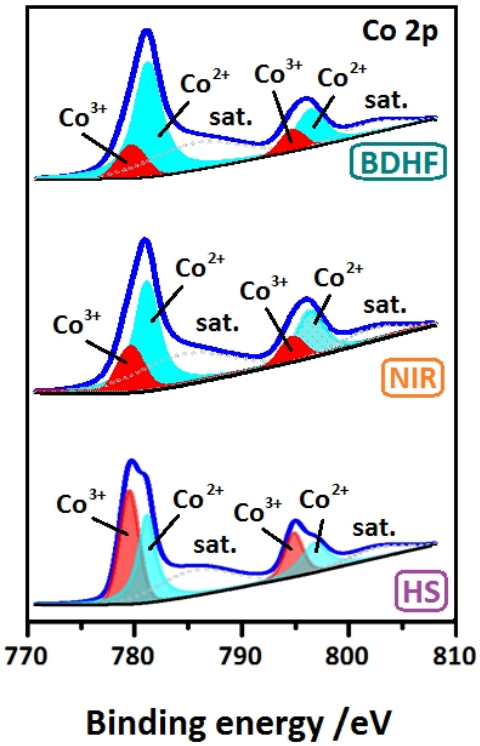

Figure S3 Co2p XPS spectra of the DBHF (top), NIR (middle) and HS (down) samples.

Figure S4

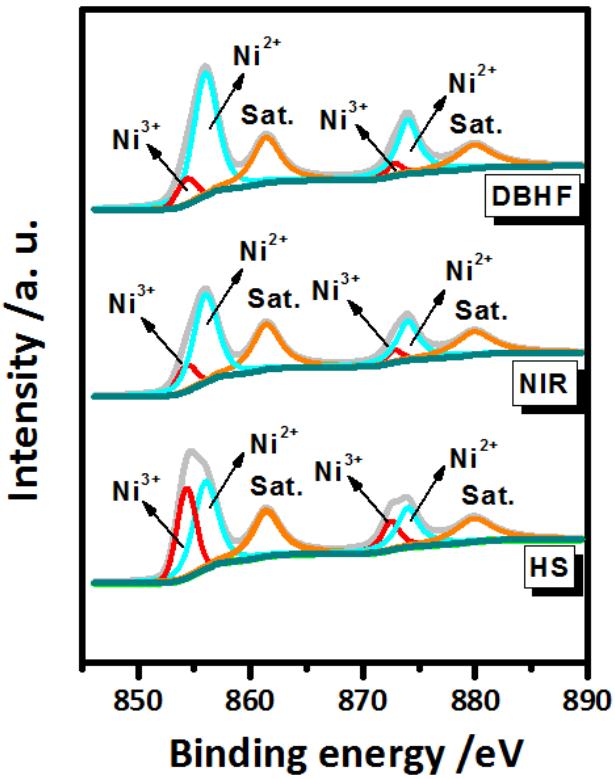

Figure S4 Ni2p XPS spectra of the DBHF (top), NIR (middle) and HS (down) samples.

Figure S5

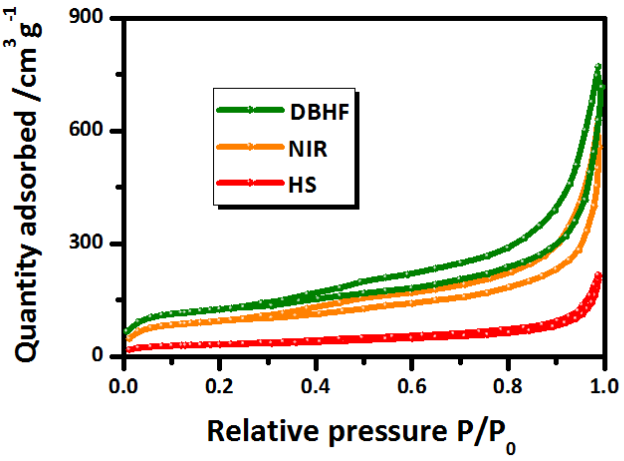

Figure S5 Nitrogen sorption isotherms of the DBHF, NIR and HS samples.

Figure S6

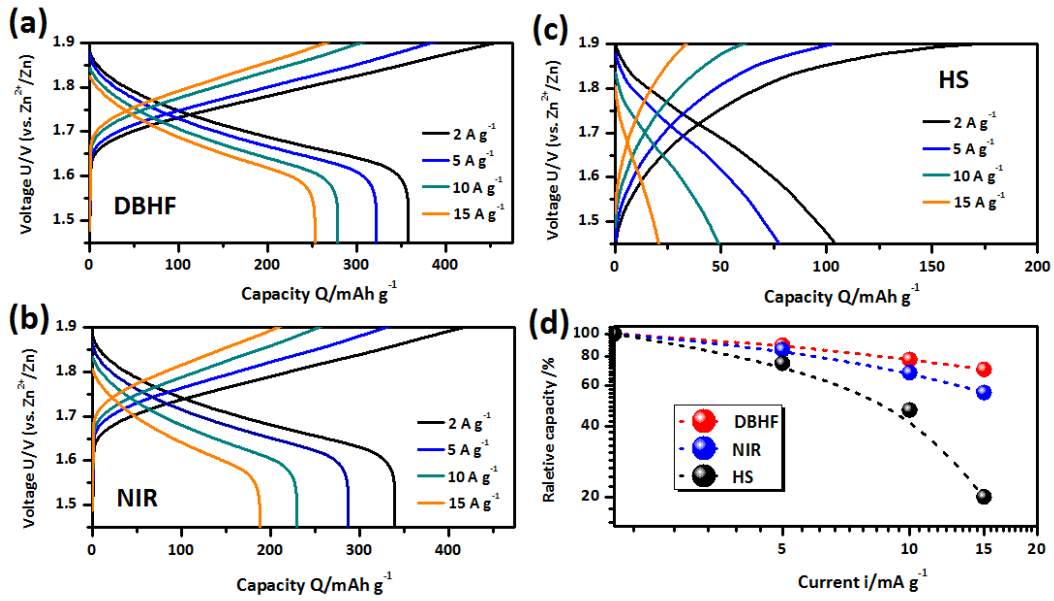

Figure S6 (a~c) Discharge curves of (a) DBHF, (b) NIR and (c) HS samples at the current densities of 2 A g^{-1}, 5 A g^{-1}, 10 A g^{-1} and 15 A g^{-1}. (d) The comparison of the relative capacities of all the samples at different current densities. The relative capacity is calculated based on the ratio of the capacity at a certain current density to the capacity at the 2 A g^{-1}. All the current densities and the capacities are calculated based on the mass of $NiCo_2O_4$ active materials in the electrodes.

Figure S7

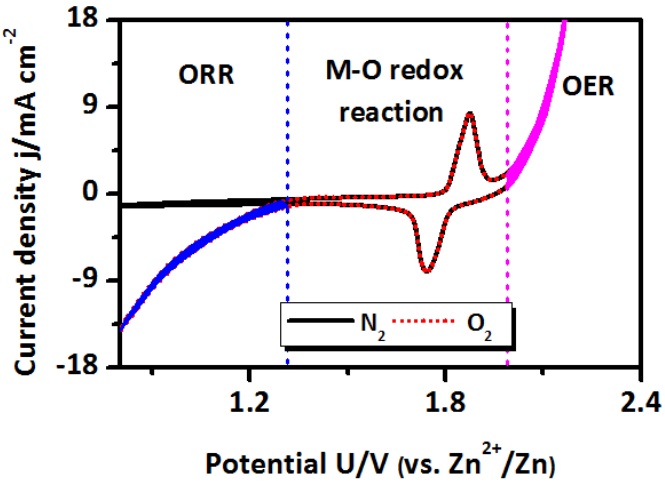

Figure S7 CV curves of the prepared HZB with DBHF cathode in the N_2 or O_2-saturated environments.

Figure S8

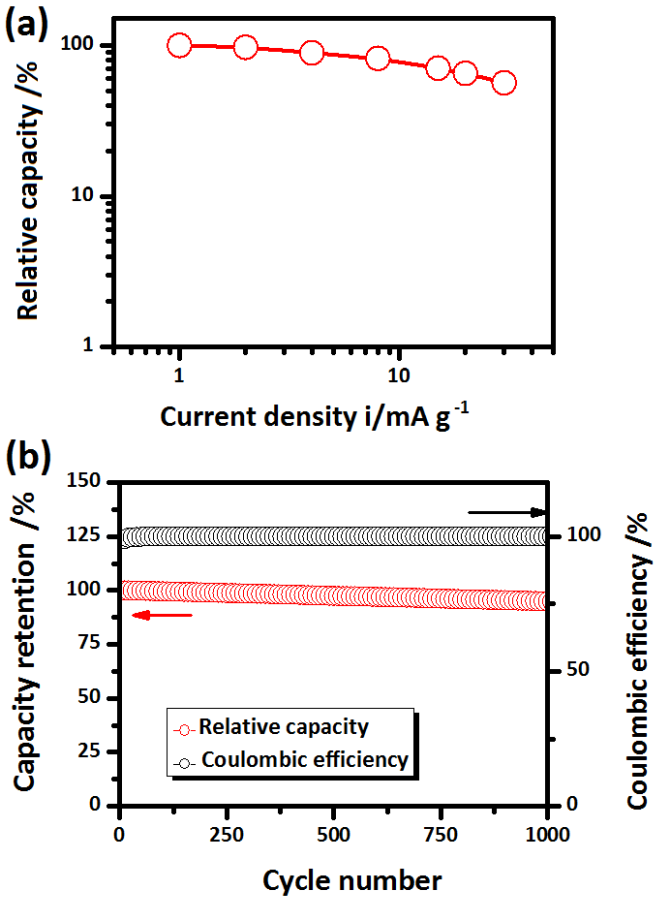

Figure S8 (a) Rate capability and (b) long-term cycling property of the hybrid Zn battery with DBHF cathode in the air-free working condition. In a, the relative capacity is the ratio of the capacity at a certain current to that at 1 A g^{-1}. In b, the capacity retention is calculated based on the ratio of the capacity in a certain cycle to that in the initial cycle.

Part II: Supporting Tables

Table S1 ORR activities of the non-noble catalysts in recent publications

Materials	Half wave potential (V vs. RHE)	Limiting current density ($mA\ cm^{-2}$)	Refence
N-doped $NiCo_2O_4$	063	5.0	S3
$NiCo_2O_4$/graphene	0.665	4.5	S4
$NiCo_2O_4$/C	0.71	6.0	S5
$NiCo_2O_4$ hollow	0.67	5.7	S6
$NiCo_2O_4$-NG/C	0.765	5.7	S7
$NiCo_2O_4$ nanosheet	0.74	5.2	S8
$NiCo_2O_4$/hollow carbon spheres	0.78	5.8	S9
$NiCo_2O_4$-250	0.78	5.8	S10
$NiCo_2O_4$-CN-180	0.81	5.4	S11
DBHF sample	0.81	5.5	This work

Table S2 Slope of Tafel plots during OER process for the non-noble catalysts in recent publications

Materials	Slope of Tafel plot ($mV\ dec^{-1}$)	Refence
$NiCo_2O_4$/NIF	106	S12
$NiCo_2O_4$/graphene	94	S4
$NiCo_2O_4$/C	78.7	S5
$NiCo_2O_4$ nanosheet	75	S8
N-doped $NiCo_2O_4$	74	S3
$NiCo_2O_4$/FTO	54	S13
$NiCo_2O_4$-CN-180	53.5	S11
DBHF sample	55	This work

Part III: Supporting references

[S1] Y. Huang, Z. Li, Z. X. Pei, Z. X. Liu, H. F. Li, M. S. Zhu, J. Fan, Q. B. Dai, M. D. Zhang, L. M. Dai, C. Y. Zhi, Adv. Energy Mater. 2018, 8, 1802288.

[S2] Z. D. Huang, X. L. Li, Q. Yang, L. T. Ma, F. N. Mo, G. J. Liang, D. H. Wang, Z. X. Liu, H. F. Li, C. Y. Zhi, J. Mater. Chem. A 2019, 7, 18915.

[S3] J. Bian, X. Cheng, X. Meng, J. Wang, J. Zhou, S. Li, Y. Zhang, C. Sun, ACS Appl. Energy Mater. 2019, 2, 2296-2304.

[S4] S. Jiang, K. Ithisuphalap, X. Zeng, G. Wu, H. Yang, J. Power Sources 2018, 399, 66-75.

[S5] J. Wang, Z. Wu, L. Han, R. Lin, H. L. Xin, D. Wang, ChemCatChem 2016, 8, 736-742.

[S6] J. Wang, Y. Fu, Y. Xu, J. Wu, J. H. Tian, R. Yang, Int. J. Hydrogen Energy 2016, 41, 8847-8854.

[S7] L. Wan, G. Zang, X. Wang, L. Zhou, T. Li, Q. Zhou, J. Power Sources 2017, 345, 41-49.

[S8] W. Liu, J. Bao, L. Xu, M. Guan, Z. Wang, J. Qiu, Y. Huang, J. Xia, Y. Lei, H. Li, Appl. Surface Sci. 2019, 478, 552-559.

[S9] H. Yuan, J. Li, W. Yang, Z. Zhuang, Y. Zhao, L. He, L. Mai, ACS Appl. Mater. Interfaces 2018, 10, 16410-16417.

[S10] J. Zhao, Y. He, Z. Chen, X. Zheng, X. Han, D. Rao, Y. Deng, ACS Appl. Mater. Interfaces 2019, 11, 4915-4921.

[S11] Y. Li, Z. H. Zhou, G. Cheng, S. B. Han, J. L. Zhou, J. K. Yuan, M. Sun, L. Yu, Electrochim. Acta 2020, 341, 135997.

[S12] L. Yang, B. Zhang, B. Feng, L. Feng, Chem. Comm. 2018, 54, 13151-13154.

[S13] J. He, Y. Sun, M. Wang, Z. Geng, X. Wu, L. Wang, S. Feng, J. Alloys Compd. 2018, 752, 389-394.